npj | Materials Degradation

www.nature.com/npjmatdeg

ARTICLE OPEN

Using macro and micro electrochemical methods to understand the corrosion behavior of stainless steel thermal spray coatings

Samantha Michelle Gateman[1], Ilias Halimi[1], Alexandre Romão Costa Nascimento[2], Robert Lacasse[3], Robert Schulz[3], Christian Moreau[2], Richard Chromik[4] and Janine Mauzeroll[1]

High-velocity oxygen fuel thermal spray stainless steel coatings are desirable for their excellent erosion resistance. However, the fabrication process can lead to a decrease in corrosion resistance in comparison to the original bulk material. Here we produced stainless steel coatings on stainless steel substrates using varying deposition parameters to investigate the corrosion properties of the resulting composite steels and elucidate the corrosion behavior both on the macro and micro scale. Macro potentiodynamic polarization measurements carried out in corroding environments demonstrated the rate of degradation of the Fe-Cr alloy coating. After short immersion periods, the coatings showed iron-like active corroding behavior and no passivation regions on the anodic branch. Over time, the coating's corrosion behavior began to change to signify similar results to that of pure chromium. Ex-situ electron microscopy and elemental composition revealed a Cr oxide rich layer left on the coating's surface. Micro electrochemical techniques including scanning electrochemical microscopy and scanning micropipette contact method were employed over the coatings and powdered material, respectively, to show that the lack of protective passivity the thermal spray coatings possess is mostly inherited from the atomized powdered stainless steel material.

npj Materials Degradation (2019)3:25 ; https://doi.org/10.1038/s41529-019-0087-0

INTRODUCTION

The success of the renewable/non renewable energy divisions, and other industrial sectors including aerospace and automotive, is significantly owed to the advancement of spray coating technologies as these coatings are essential for maintaining functionality, safety, reliability and increasing the lifetime of expensive components and machinery.[1,2] As an example, some Canadian hydropower equipment has been in service for more than 100 years because of the use of erosion mitigating technologies such as thermal spray coating methods and their ability to extend performance.[3] While the erosion resistance of machinery has been improved, water contamination and infiltration can lead to severe damage and reduced operating life through corrosion mechanisms and other relevant processes.

To limit corrosion in aqueous environments, thermal spray coatings often have a high content of corrosion resistant stainless steels (SS).[4,5] SS are ferrous alloys with chromium (>12 wt%)[6] added to encourage the formation of a Cr rich oxide film over the metals surface, known as a passive film, which protects the bulk material from further degradation.[7] For bulk SS alloys, film breakdown or damage exposes active metal, creating a localized vulnerable site to the oxidizing environment and with chloride present can lead to localized corrosion.[8] This type of corrosion can be evaluated by using the bulk electrochemical technique of potentiodynamic polarization (PDP), where a sudden increase in current density during an anodic scan indicates a breakdown in the passive film. The potential at which this occurs, defined as the pitting potential (E_{pit}), is a measure of how susceptible a material is to localized corrosion. However, the sample preparation for recording E_{pit} usually includes an intensive polishing regime prior to electrochemical measurements, producing specimens with a mirror-like finish.[9] This creates a smooth surface where the oxide film can uniformly grow across the metal's exterior, usually indicated by a more noble corrosion potential, E_{corr}. In contrast, thermal spray coatings are known for their high surface roughness, porosity, complex microstructure, and unique composition,[10,11] making it difficult to study the material's corrosion behavior using solely time-dependent macro electrochemical measurements. It has been previously reported that thermal spray coatings do not hold the original corrosion resistance of a bulk SS alloy when comparing PDP measurements using the ASTM standard due to the significantly modified microstructure and composition of the sprayed coatings.[5,11] However, it was not well understood which aspect of the microstructural modification was primarily responsible for the performance gap and which step in the coating fabrication process is responsible for this.

The manuscript presented describes the power of combining both macro and micro electrochemical methods in order to fully understand the corrosion behavior of thermal sprayed coatings. The macro PDP measurements of thermal sprayed coatings described in this work have been performed on "as sprayed" specimens. This is because such coatings are not prepared via abrasion and/or polishing prior to implementation in their

[1]Laboratory for Electrochemical Reactive Imaging and Detection of Biological Systems, McGill University, Montreal QC H3A 0B8, Canada; [2]Thermal Spray and Multiphase Flow Laboratory, Concordia University, Montreal QC H3G 1M8, Canada; [3]Institut de recherche d'Hydro-Québec, Varennes J3X 1S1, Canada and [4]Mining and Materials Engineering, McGill University, Montreal QC H3A 0C5, Canada
Correspondence: Janine Mauzeroll (Janine.mauzeroll@mcgill.ca)

Received: 12 February 2019 Accepted: 16 May 2019
Published online: 14 June 2019

Published in partnership with CSCP and USTB

npj nature partner journals

respective applications and hence is a more realistic analysis of the materials corrosion behavior. The combination of macro and micro electrochemical techniques has been previously reported for the bulk SS 444 Ti and Nb stabilized alloy, using both PDP and scanning electrochemical microscopy (SECM) to expose the initiation sites of localized corrosion.[12] To our knowledge, SECM has only been exploited once before in the thermal spray community, where it was used to study a Ni based alloy (Inconel 625) thermal spray coating to measure the kinetic rate constant of a redox mediator across the coating's heterogeneous microstructure.[13] The work described here combines both macro and micro electrochemical methods along with electron microscopy to provide insights into the corrosion behavior of thermal sprayed SS coatings of industrial relevance.

RESULTS

Bulk characterization of thermal spray coatings

SEM images of the polished bulk SS 444 and the coating's microstructure can be seen in Fig. 1a, b, respectively. The bulk material is known for its resistance to localized corrosion, exceeding the performance of 300 series SS such as SS 316 and 304.[14] The alloying elements Ti and Nb precipitate out with parasitic amounts of carbon and nitrogen to form chemically stable Ti/Nb nitride and carbide inclusions, which keeps Cr in solid solution for passive film formation. Bulk SS 444 shows such Ti/Nb stabilizing inclusions uniformly distributed across grains about 50.71 ± 9.36 µm in diameter (Fig. 1a), with an inset of a TiN inclusion 5 µm in size. The grain size was determined using the line intercept method of ten different lines across the SEM image via ImageJ software. It is important to note the distinct inclusions found within the bulk sheet material, as their presence in the manufactured powder SS is crucial for corrosion resistance.

The thermal spray coatings were produced using a water atomized SS 444 powder. The particle velocity and temperature within the thermal spray gun were varied between 550-800 m/s and 1600–2100 °C, respectively, to produce 4 distinct high-velocity oxygen fuel spray (HVOF) coatings (Figure S1A). HVOF was selected as the fabrication technique because it is known for producing hard and dense coatings, providing protection against erosion. The coating produced at high particle velocity and low temperature (HVLT in Figure S1A) is used as the example coating for the rest of the paper as the parameters used were similar to those implemented for the SS 316 coating. The cross section of the thermal spray coatings imaged using BSE-SEM exposes its oxidized particle layered structure, where the bright zones are bulk SS 444 particles and the darker areas are oxidized metal formed in flight during the coating fabrication process (Fig. 1b). Unlike the bulk metal (Fig. 1a), no micron sized Ti/Nb rich inclusions were observed via SEM/EDX within the thermal spray coatings.

The existence and stability of a protective passive film can be observed and measured electrochemically using bulk PDP measurements. The corrosion potential, E_{corr}, of the bulk material is very noble at a value of -0.12 ± 0.01 V vs. SCE as seen in Fig. 1c. The cathodic branch is activation controlled potentially due to the presence of the Ti/Nb inclusions, which remain uncovered by the passive film and hence act as local reduction sites.[12] Such cathodic Tafel behavior has been documented for TiN films previously.[15,16] The anodic branch, however, plateaus at a limiting current density, or j_{lim}, of 0.50 ± 0.02 µA/cm^2, indicating that the anodic reaction is diffusion controlled due to the presence of the passive film.[17] Sources of error during PDP measurements include small variations in: the immersion time the samples endured before starting the measurement, the concentration of the electrolyte, and in the samples themselves. The breakdown potential of the material is extremely noble, measured to be 1.09 V vs. SCE (Figure S2). This is characteristic of reaching the transpassive potential where the Cr-rich oxide passive film is oxidizing and/or oxygen evolution is occurring.[12] The diffusion limited anodic current density combined with the noble E_{corr} and breakdown potential confirms that the passive film is present and protective on the bulk SS 444.

In contrast, all PDP curves measured on the fabricated SS 444 HVOF coatings show a more active E_{corr} with an example PDP measurement in Fig. 1c with a value of E_{corr}: -0.46 ± 0.05 V vs. SCE. The cathodic branch is under diffusion controlled polarization, probably due to the formation of corrosion product, which hinders the electrochemically active species access to the electrode's surface. Furthermore, the anodic branch does not show passivation, but indicates that the coating is undergoing activation controlled polarization due to the consistent increase in current density. The coating produced using low velocity and high particle temperature (LVHT, Figure S1) had a significantly different E_{corr} of -0.55 ± 0.07 V vs. SCE after only 1 hr immersion in comparison to the rest of the fabricated coatings (Figure S1B). In order to investigate why, immersion PDP measurements were utilized in the proceeding section.

The SS 444 HVOF coatings also show a larger corrosion current density (j_{corr}) with a value of 15.1 ± 0.4 µA/cm^2, which is dependent on the geometric surface area exposed during the PDP. Although the current is divided by the exposed surface area of the substrate (1 cm^2), the surface roughness of the coating is greater than the polished bulk material and therefore may contribute to the shift to a larger corrosion current density. Profilometry measurements (Figure S3) performed across a polished sheet SS 444 sample as well as an as sprayed SS 444 HVOF coating revealed a mean height, or S_a, of 0.01 and 13.52 µm, respectively. Nonetheless, the ~2-order of magnitude increase in j_{corr} for the coatings cannot only be attributed to the increase in surface area due to the similar corrosion rates measured for polished pure metallic Fe (Fig. 2b). Therefore, the reactivity of the coatings indicate an increase in corrosion rate in comparison to the bulk SS 444 metal.

Polarization immersion test

PDP measurements were performed under aerated conditions and using the ASTM standard protocol for ferrous metals.[18] This involves a 1 hr incubation period of the sample at open circuit potential (OCP) to measure the E_{corr} prior to the PDP. However, the SS 444 coatings actively corroded during the 1 h PDP measurement, indicating the lack of a protective passive film present on the coating's surface and/or surface chemical changes. Since SS 444 is mainly a Fe-Cr alloy, one element in the coating may be oxidized while the other remains protected, similar to the dealloying of Zn from CuZn alloys.[19,20] Over time, the precedence of corrosion of one alloyed element may become so strong that a change in chemical composition of the remaining coating could be observed.

Immersion of SS 444 coating

A SS 444 coating was repetitively analyzed using PDP measurements at increasing immersion times (Fig. 2a). The measured E_{corr} decreased by 250 mV after ~100 h of immersion. In contrast, the anodic Tafel slope changed from being active to showing a passivation region. Similar electrochemical behavior was observed for HVOF coatings that were immersed and then measured without applying multiple PDP measurements (Figure S4). The sample was analyzed using SEM/EDX and near-IR laser Raman spectroscopy before and after the PDP immersion tests to observe the change in the coating's morphology and chemical composition. Molten SS 444 powder particles can be seen across the as sprayed rough thermal spray surface in Fig. 2c as outlined in white dotted line circles. After accelerated corrosion testing, the powder

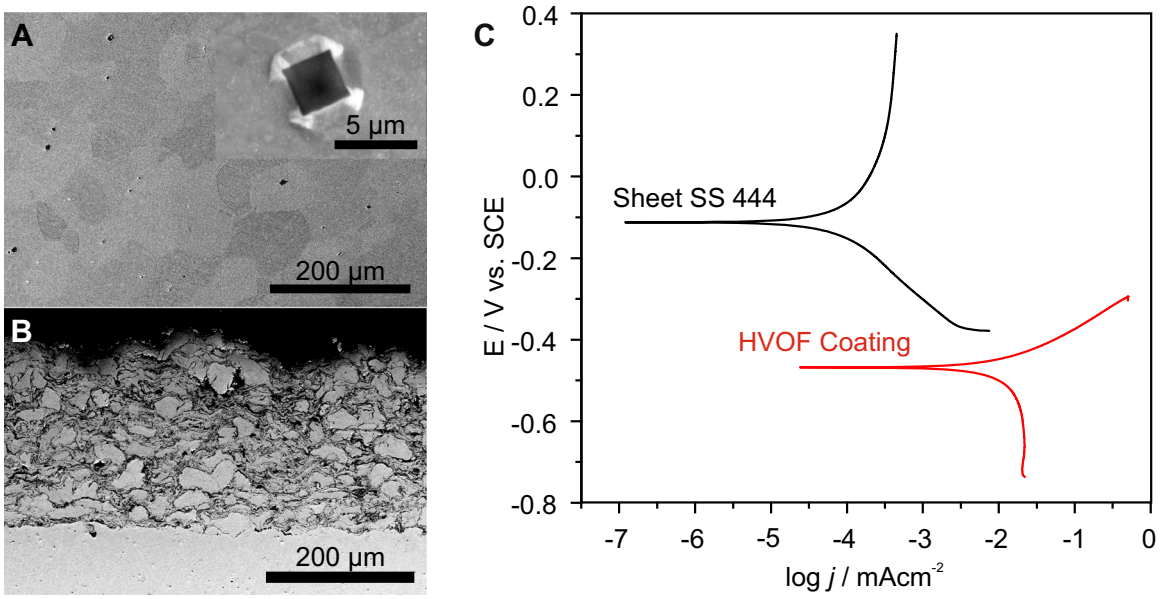

Fig. 1 **a** SEM images of the bulk sheet metal's microstructure including the Ti/Nb rich inclusions (inset) and **b** the polished cross-section of the thermal spray coating using BSE-SEM. **c** Potentiodynamic polarization measurements of sheet SS 444 and HVOF coating SS 444 in 3.5 wt% NaCl

particles become hollowed out to leave a shell-like structure on the surface of the coating as seen in Fig. 2d. The enhancement of Cr and oxygen on the surface of the corroded sample was observed via EDX point analysis (Figure S5). The [Cr]/[Fe] ratio increased from 0.23 to 0.39 after immersion, showing a significant Cr enrichment compared to both the as sprayed coating and the original composition of the SS 444 alloy ([Cr]/[Fe] ratio of 0.22 as described in Table 1). The Raman spectrum of the as sprayed SS 444 coating revealed an oxide composition of mainly α and γ-Fe_2O_3 phases, hematite (trigonal) and maghemite (cubic), respectively, formed during the thermal oxidation of the particles throughout the spray process (Figure S6A).[21] After 100 h of immersion, the Raman spectrum correlates to a few types of Fe hydroxides including α- and γ-FeOOH[21] as well as Cr_2O_3[22,23] as seen in Figure S6B, indicating a chemical compositional change during long time immersion testing.

PDP of pure elements

In order to compare the coatings electrochemical behavior at different immersion times to pure metallic Fe and Cr, samples of each were prepared and analyzed using PDP and can be seen in Fig. 2b. The E_{corr} of Fe and Cr were −0.45 and −1.09 V vs. SCE, respectively. Although Fe is more noble, the anodic branch of the PDP shows active corrosion whereas the Cr protectively passivates.

Immersion of SS 316 coating

A similar measurement was performed on another type of SS HVOF coating, SS 316, to observe the change in electrochemical and chemical properties of a Ni containing SS coating after long time immersion. After the first 1 hr PDP, the SS 316 HVOF coating was immersed for 1 month before performing the next PDP measurement. The resulting PDP measurements show a drop in corrosion potential from −0.53 to −0.81 V vs. SCE and a small region of passivation (Figure S7). When the electrochemical cell was dismantled, the entire coating delaminated from the substrate (Figure S8A). Ex-situ SEM analysis showed that this type of coating also suffered from a change in morphology as grains of the SS powdered metal have been etched away with grain boundaries remaining (Figure S8B). Since Fe readily dissolves during these experiments, this shows that the oxidized film is not protectively passivating the coating's surface and allows for the active corrosion of Fe-rich regions. Over time, the amount of Fe will decrease, leaving Cr rich material across the coating's surface and hence why a passivation region from −0.70 to −0.80 V is seen after one month.

Probing passivity of coatings using SECM

SECM is a scanning probe technique that allows for spatiotemporal resolution of electrochemical reactivity on the nano and micro scale. The feedback mode of SECM was used in order to probe the redox mediator's that is, ferrocene methanol's (FcMeOH), reactivity across the thermal spray's surface using a 4.7 µm diameter carbon ultra microelectrode (UME) (Figure S9B). The current map collected of the regenerated redox mediator from the face-on abraded and polished SS 444 coating can be found in Fig. 3a. The nature of the current measured during the feedback measurements is mostly from the ability of the redox mediator to regenerate at the coating's surface and be collected at the UME's tip to form a feedback loop. The stability of the UME and the redox mediator over the course of the experiment was measured using cyclic voltammograms (Figure S9A). Comparing the SEM and SECM images in Fig. 3, the SS 444 particles appear to generate a smaller flux than the surrounding oxidized regions.

By recording the current measured at the tip of the UME while approaching the coating along the *z*-axis, the local reactivity of FcMeOH, and hence the substrate, can be measured. It has been previously shown that a probe approach curve (PAC) over an unbiased, prepared bulk SS 444 substrate obtained over the passive film displays almost pure negative feedback as seen in Fig. 3c in red, which confirms the insulating behavior of the non-polarized passive film formed.[12] In contrast, the PACs recorded over multiple areas of the coating can be seen in red in Fig. 3c. The entire coating's surface measured positive feedback indicating the materials activity on the micro-scale and with respect to the tip size of the UME. Furthermore, the degradation of the coating due to corrosion can be observed around the probed area (Figure S10) indicating the lack of passivation layer.

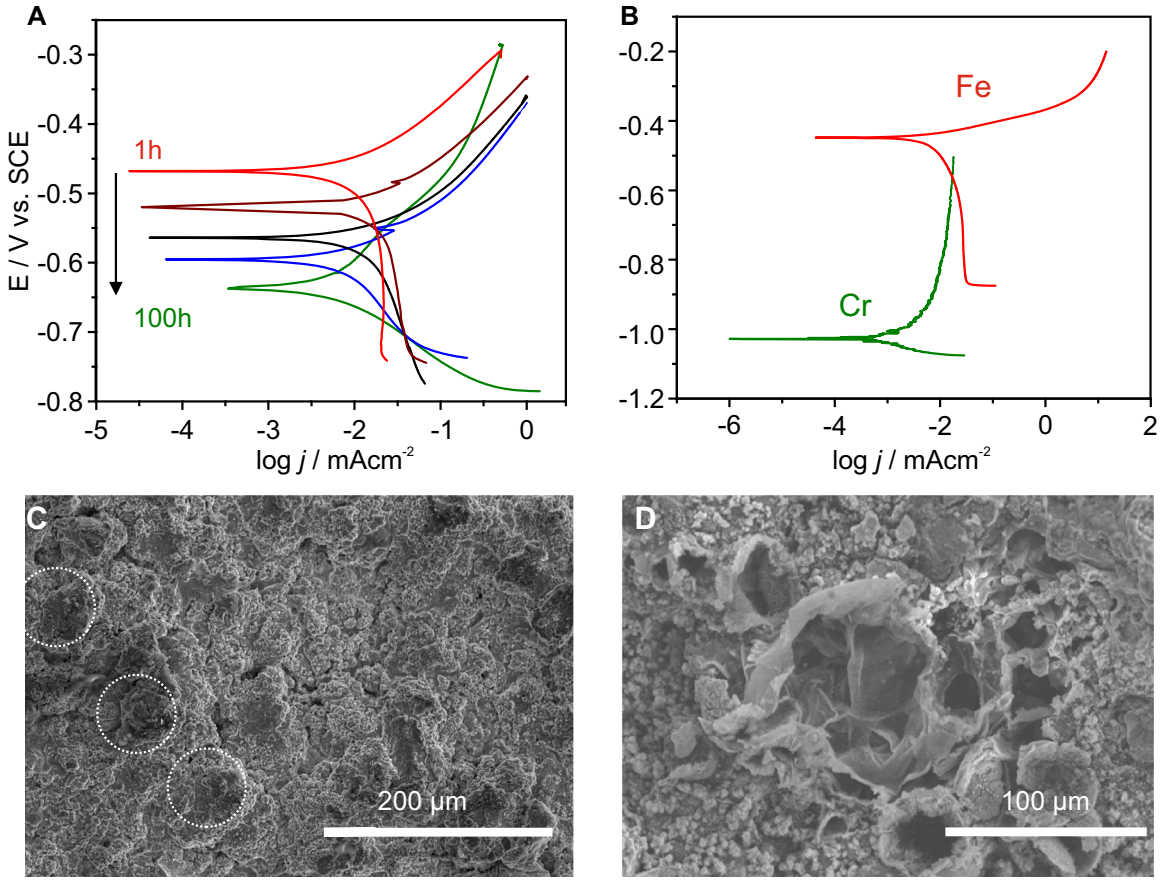

Fig. 2 **a** PDP measurements of a SS 444 HVOF coating recorded at increasing immersion times from 1 h (red), 5 h (wine), 10 h (black), 24 h (blue), and 100 h (green) show a drop in corrosion potential (black arrow) and evolution of passivity region over time. This shift in corrosion behavior can be attributed to the chemical change over time from being Fe rich to Cr rich as seen from the PDP measurements in pure metallic Fe and Cr in **b**. The SEM images of the coatings before (**c**) and after (**d**) immersion tests show the loss of material and shell-like morphology of the corroded coatings

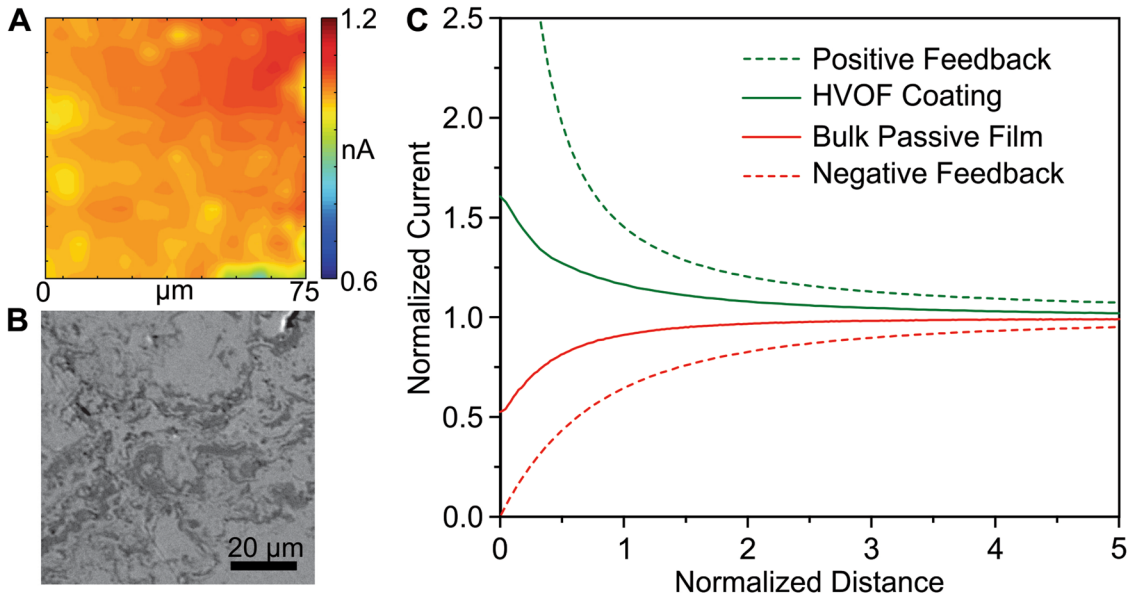

Fig. 3 **a** SECM current map recorded 5 µm above the surface of (**b**) a polished SS 444 thermal spray coating indicating sites of dampened reactivity over SS particles and increase in reactivity over the oxide interconnecting regions. **c** SECM approach curves show positive feedback over all sites investigated across the coating (solid green) in contrast to the negative feedback measured over the bulk SS passive film (solid red). Theoretical positive and negative feedback are presented for comparison

Characterization of powder SS 444

The lack of Ti/Nb stabilizing inclusions and protective passivity measured for the coatings leads us to investigate the coating's starting material, the atomized water quenched SS 444 powder.

ICP-OES of powder SS digestion

The SS 444 powder was digested in aqua regia at elevated temperatures to prepare the sample for elemental composition quantification. Even after 24 h of digestion, the sample did not fully dissolve under such harsh conditions. This is dissimilar to what was found for the bulk sheet SS 444 material, as this metal completely dissolved under the same conditions. The insoluble material was filtered, collected, cleaned, and dried under air for further analysis. The digested SS 444 powder sample was further diluted and analyzed using inductively coupled plasma optical emission spectroscopy (ICP-OES). The average wt% of each quantifiable element can be seen and compared with the results for the fully digested bulk SS 444 in Table 1. The overall wt% of Fe and Cr measured in the powder SS was significantly lower than the amount found in the bulk metal. It can be noted that the total wt% of the powder sample is far from summing to 100%. This is due to the insoluble material not being available for analysis by ICP and the inability to quantify Ti, Nb, and Si while using a glass nebulizer as these elements required dissolution in HF.

The insoluble material was analyzed using SEM/EDX to reveal its morphology and chemical composition. A hollowed out powder particle with a shell-like structure can be observed in Figure S11A, with small ~2–5 µm pores present and scattered across its exterior. The insoluble particle shells were found to be rich in Cr, O, and C, while low in Fe wt% in comparison to the bulk material (Figure S11B) with a [Cr]/[Fe] ratio of 4.41. This Cr-rich surface oxide layer is similar to what remained after the PDP immersion tests presented in Section 2.2 and is speculated to be Cr_2O_3 as this material does not readily dissolve in acid. This evidence suggests a bi-phasic composition of the powdered material. In spite of the formation of this Cr-rich shell surrounding the atomized powder particle, the bulk composition of the particle remain essentially the same as that of the bulk SS 444 in terms of Cr content as indicated by the [Cr]/[Fe] ratios shown in Table 1.

Bulk PDP of powder pellets

The corrosion properties of the powdered SS 444 metal were investigated by fabricating pellets and using PDP measurements. The pellets measured an E_{corr} ~ 100 mV more active than an average thermal spray coating. Furthermore, the pellets show a 1.5 order of magnitude increase in corrosion current density to the presented coatings even after correcting for the exposed surface area. These results indicate that the powder pellets are more active than the SS 444 coatings and bulk sheet metal using bulk electrochemical techniques.

Etched SS 444 powder particle

The microstructure of the powdered SS 444 was observed using SEM/EDX. Powder particles were sprinkled into an insulating epoxy resin and abraded/polished to expose the powder's microstructure. The prepared sample was then etched using 10:1:10 vol. ratio of HCl:HNO_3:H_2O for 30 s and then rinsed and dried for analysis. Figure 4b shows an electron micrograph of an etched powder particle with an estimated ferritic grain diameter of 3.06 ± 0.45 µm as measured using ImageJ and the line intercept method. Upon further investigation using EDX linescans, irregularly shaped Cr rich inclusions 0.5–2 µm in diameter are observed to have precipitated out with silicon and oxygen (Fig. 4c). Depletion of Cr surrounding the inclusions was not detected. In contrast, stabilizing Ti/Nb rich inclusions were not located in either powder particles nor as separated individual inclusions during this analysis.

Table 1. ICP-OES average wt% measurements of each element in bulk and powder SS 444 digested samples and associated standard deviations to nine samples

Element	Bulk SS wt%	Powder SS wt%
Fe	79.54 ± 7.81	64.70 ± 11.32
Cr	17.30 ± 2.60	14.15 ± 2.92
Mo	1.93 ± 0.13	1.78 ± 0.20
Ni	0.25 ± 0.01	0.25 ± 0.03
Mn	0.30 ± 0.01	0.13 ± 0.01
V	0.11 ± 0.01	0.08 ± 0.01
Cu	0.08 ± 0.07	0.11 ± 0.02
Total	99.51 ± 8.23	81.12 ± 11.69
[Cr]/[Fe]	0.22	0.22

Single particle PDP measurements

In order to measure individual particle's corrosion behavior to avoid effects due to the porosity of sintered pellets, the scanning micropipette contact method (SMCM) was employed on a single SS 444 powder particle and various micro PDP measurements were collected. SMCM consists of a two electrode setup inside of a micropipette as seen in Fig. 5a, where the material of choice is employed as the working electrode and the quasi reference/counter electrode is inserted into the back of the micro cell. As seen in Fig. 5b, c, the silanized micropipette's aperture is 500 nm in diameter, which is much smaller than the average size of a SS 444 particle (~45 µm) and the pores found across the Cr oxide shell (1–5 µm). Once contact between the two electrodes is made, a micro PDP measurement can be performed before retracting the micropipette and moving the cell to another position on the particle. The micropipette was moved in 1 µm increments to ensure the measurements were performed on the same particle. The measurements were performed on full powder particles possessing oxide shells. Both active and passive corrosion behaviors were observed over the same particle, measuring an E_{corr} of −0.42 ± 0.01 V (similar to those of coatings) and −0.15 ± 0.03 V (Close to that of wrought SS 444) vs. SCE, respectively in Fig. 5d. These results agree with the insoluble material observed after chemical digestion; where the Cr oxide shell protects some regions across the powder particle while other areas are more susceptible to corrosion due to the porosity of its exterior.

DISCUSSION

Regardless of the spray parameters used, the SS based HVOF coatings demonstrated active corrosion rather than passivation, even though the ICP-OES results measure Cr content over the defined threshold of 12 wt%.[6] The difference in chemical composition of the coatings before and after long-term immersion was shown both by EDX and electrochemical PDP of pure metallic Fe and Cr. The thermal spray coatings show similar corrosion properties to pure Fe after 1 h immersion in 3.5 wt% NaCl electrolyte. At neutral pH, the Fe oxide formed is not protective and thus the pure metal actively corrodes. After days of exposure, the coatings begin to show passivating behavior, similar to that of pure Cr. The difference in PDP behavior between the more active coating (LVHT) and the others fabricated during this work could be explained by the material's increase in Cr oxidation from using a high particle temperature and low velocity. Using such parameters gives the particles more time to oxidize Cr in flight

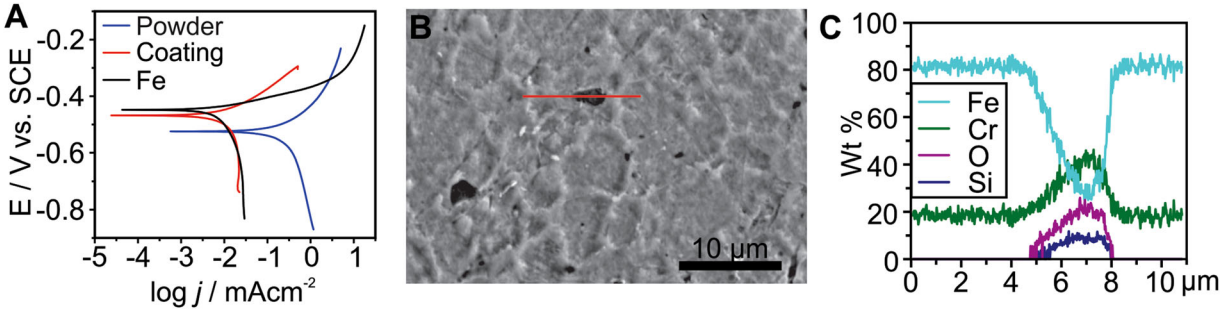

Fig. 4 **a** The SS 444 powder pellets were characterized using PDP measurements to observe the materials corrosion properties. The corrosion behavior of pure Fe and a SS thermal spray coating are presented for comparison. **b** A SEM image of a SS 444 powder particle that was polished and etched to reveal its microstructure. **c** EDX linescans show the presence of Cr rich inclusions

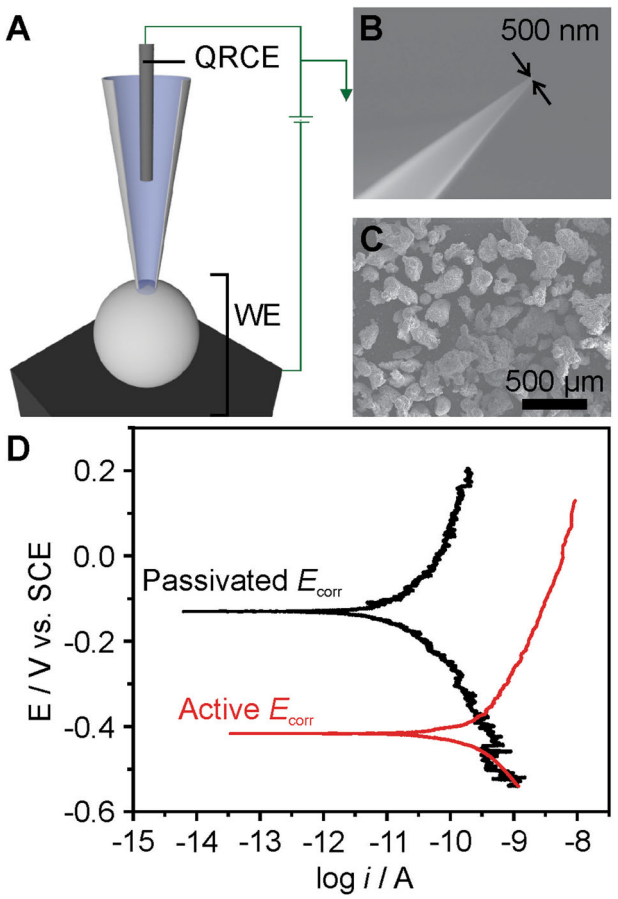

Fig. 5 **a** schematic of the SMCM setup used to perform micro PDP measurements on individual SS 444 powder particles. **b** SEM image of a silanized micropipette tip with a diameter of 500 nm. **c** SEM image of SS 444 powder particles dispersed across carbon tape. **d** Example micro PDP measurements collected over different areas of a single SS 444 powder particle, demonstrating both active and passive behavior

and segregate from the Fe matrix. Consequently, this coating undergoes Fe dissolution at a faster rate than the rest of the thermal spray coatings. This behavior cannot be extracted from single OCP or E_{corr} measurements over time,[5] nor from other long term immersion tests such as salt spray corrosion testing,[1,24] and therefore demonstrates the power of utilizing long time immersion PDP measurements.

The micro electrochemical investigation of the HVOF SS 444 coatings via SECM revealed the reactivity of the oxide strings and the SS particles. The approach curves show positive feedback indicating the lack of passivity at the resolution of the UME used. After the experiment, uniform corrosion can be found in the surrounding probed area. This is different to the SECM experiments performed on bulk sheet SS 444, where the presence of the passive film is indicated by negative feedback and the material is highly stable over long immersion and testing times.[12]

The filtration and characterization of insoluble material after acid digestion of the powder SS 444 reported here agrees with the previous surface chemical analysis performed on Cr alloyed steel particles,[25] that the particles possess a Cr oxide rich shell after powder fabrication and before production of coatings. The presence of 2–5 µm pores in the non-protective shell are comparatively the same size and shape as the powder's ferritic grains exposed via chemical etching, raising the speculation of grain-dropping corrosion mechanisms. This grain-dropping corrosion pattern could suggest intergranular corrosion, where Cr carbide inclusions leave the adjacent surrounding metal matrix Cr depleted and unable to repassivate[26] although no such depletion was detected in the present work. More likely, the Cr rich inclusions found to precipitate out of the metal particle's matrix with Si and O during the atomization process enhance vulnerability of the metal to locally corrode via a micro galvanic corrosion mechanism and hence enable the active degradation of the rest of the particle. The fabrication and utilization of carbon nano electrodes to investigate the local reactivity of powder particles via SECM is currently ongoing.

The stabilizing Ti/Nb rich inclusions were not observed within the SS 444 coatings nor the powdered metal, which may play a role in the material's decrease in corrosion resistance by not being present to precipitate out with carbon and/or nitrogen. In order to fabricate powdered SS, the cast metal was melted at a temperature above the alloy's melting point (~1500 °C).[27] However, the melting point of Ti/Nb carbides and nitrides are much higher (+3400 °C)[28] and therefore could have remained solid during the melting process. The unmelted inclusions, 5–10 µm in size,[12] are smaller than the average particle diameter of the SS powder used in this study (~45 µm) and hence could have been excluded from the as sprayed powder during sieving after atomization. No Ti/Nb rich inclusions were observed in as sprayed samples and any Ti/Nb located in the coatings were found within the oxide regions, unable to protect the SS metal matrix from possible Cr precipitate formation.[26,29]

Another alloying element commonly found in SS is Mo, known to enhance material's corrosion resistance to localized corrosion.[30,31] The Mo wt% found in the bulk metal compared with the powder material measured using ICP-OES is about the same with 1.93 and 1.78 wt%, respectively. However, the coatings and sintered powder pellets showed significant decrease in corrosion resistance. It has been proposed previously that Mo acts as a barrier element between Ti/Nb stabilizing inclusions and the metal

matrix for the SS 444 bulk metal by precipitating Nb out of solid solution.[12] However, no Mo was found to enrich the barrier sites between the Cr rich inclusions and the metal matrix within the powdered SS 444. This may be due to the lack of Nb found within the powdered material.

The resemblance of the macro corrosion behavior of the sintered powdered SS 444 pellets to pure Fe indicates the lack of a protective passive film and the presence of active degradation. The corrosion current density of the sintered pellets was higher than both the values for polished Fe and HVOF SS 444 coatings. This increase in current density may be due to the porosity the sintered pellets possess, as demonstrated for Inconel 625 powder systems.[11]

Ahmed et al. studied Ni-based alloy thermal spray coatings' corrosion behavior to investigate the performance gap between the coatings and the bulk metal.[11] The presence of Cr oxide in as sprayed coatings led to the hypothesis that the main factor in coating degradation is galvanic corrosion of localized Cr-depleted zones, assuming the Cr consumption occurred during in-flight oxidation/coating deposition process. The conflicting surface chemical analysis of Cr alloyed steel powder using X-ray photoelectron spectroscopy (XPS) and Auger electron spectroscopy by Karlsson et al. revealed that although Cr is enriched in the surface oxide, no significant depletion of Cr from the matrix owing to this enrichment was observed, thus the corrosion of such material must include another mechanism.[25] Furthermore, for various SS coatings prepared using cold spray methods where coatings are fabricated under high pressure and lower temperature conditions, the material still actively corrodes, suggesting an intrinsic issue with the SS powder starting material rather than the oxidation via coating processes.[32–34]

The utilization of SMCM resulted in obtaining the corrosion properties of an individual SS 444 particle. Both active and passive E_{corr} values can be found at different sites across the same particle. This behavior is in agreement with the morphology of the insoluble material, where parts are corrosion resistant while others are susceptible to corrosion. Therefore, the Cr passive layer does not uniformly protect the powder SS 444 particles and the material actively corrodes in aqueous environments. The corrosion of SS 316 powdered particles was studied on the micro-scale using the micro-capillary electrochemical method by Hedberg et al. where non-polished particles showed passive behavior.[35] However, the micro cell diameter used was 159 µm, almost 8x larger than the average particle size. Nonetheless, it was concluded that corrosion was not induced by bulk compositional differences but attributed to surface inhomogeneity's, similar to what has been described here.

Thermal spray coating techniques have been widely used in industry due to their ability to mitigate erosion. We have shown that although the HVOF thermal spray coating fabrication process may affect the material's corrosion properties to some extent, the protective nature of the bulk sheet material has been lost due to the powder fabrication process. Both macro and micro electrochemical techniques agreed that the SS coatings and SS powder do not passivate in a protective manner, and the formation of a porous Cr oxide shell is produced that could leave Cr depleted zones vulnerable to corrosion. Furthermore, despite the fast cooling of the atomization process, Cr rich inclusions were observed and could be capable of micro galvanic corrosion and initate pitting corrosion.

The lack of available Ti/Nb alloying elements to form stabilizing inclusions within the SS 444 grains may also have a secondary influence on the material's drop in corrosion resistance. The immersion PDP testing and comparison to the pure metals' electrochemical behavior proved to be an alternative and beneficial method for obtaining complex alloys corrosion parameters over time in order to fully understand the material's degradation behavior. The corrosion analysis performed here can be standardized and utilized to explore other complex alloyed systems to better understand their corrosion behavior and therefore predict long-term degradation performance over a lab friendly time scale.

METHODS

Sample fabrication

Thermal spray coatings. The coatings were fabricated using water atomized SS 444 powder and high velocity oxygen fuel spray coating technique on bulk SS 444. The powder was first processed using high-energy ball milling and then sieved to a mean particle diameter of ~45 µm. A Praxair's JP-8000 HVOF spray gun was used for spraying all coatings. A powder feed rate of 44 g/min, stand-off distance of 13 in (33 cm), and 15 passes were performed to create 300 µm thick coatings. The oxygen and fuel flow rates were varied to produce four velocity/temperature conditions between 500–800 m/s and 1600–2100 °C. Temperature and velocity of in-flight powders during spraying were measured with a DPV-Evolution sensor (Tecnar Automation, Saint-Bruno (Québec), Canada). The SS 316 HVOF coatings were produced using similar parameters to that of coating HVLT.

Solid powdered pellets. The powder SS 444 was transferred into a mould and pressed in order to create a solid pellet. The pellet was then sintered under vacuum (base pressure of 10^{-6} torr) at a temperature of 1000 °C for 1 h.

Bulk sample preparation. AISI grade stainless steel 444 was produced by ArcelorMittal. Iron (99.9%) and Cr lumps (99.5%) (GoodFellow Metals, Huntingdon, England) were used for pure metallic samples. All specimens were sectioned into 2 × 2 cm samples using an abrasive cutter (abrasiMet 250, Buehler, USA). Samples were fixed in cold mounting epoxy (Epofix–Struers). The SS, Cr, and Fe were ground using a series of SiC papers (800, 1200, and 4000 grit, Struers, Canada) and polished using a 0.05 µm aluminum oxide suspension and a MD Chem cloth (Struers, Canada) to obtain a mirror–like surface. All grinding and polishing procedures were carried out using a TegraPol-25 polishing wheel and an automated TegraForce-5 polishing arm (Struers, USA). All samples were sonicated in anhydrous ethanol for 2 min to remove any alumina residue, and then dried under a stream of air.

Instrumentation

SEM/ EDX analysis: All SEM images were obtained using a Hitachi SU3500 variable pressure scanning electron microscope equipped with X-ray energy dispersive spectroscopy (XEDS) (Oxford, Inca, Silicon drift detector) for micro-elemental composition determination of inclusions and secondary phases. Topographic information was obtained by collecting the secondary electron signal produced from the specimen itself while elemental composition information was explored via detection of back-scattered electrons stemming from the incident beam and x-ray emissions.

Macro potentiodynamic polarization measurements: All PDP measurements were performed using a multi-channel VSP-300 potentiostat (BioLogic Science Instruments, USA) with 1 µV resolution. Experimental parameters for PDP measurements were based on the relevant ASTM test method.[18] A standard bench top corrosion cell (K0235 Flat Cell, Princeton Applied Research, AMETEK® Scientific Instruments) with an isolated area of 1 cm^2 was used as the main corrosion cell for all measurements. A calibrated saturated calomel electrode (SCE) and platinum mesh were used as the reference and counter electrodes respectively. A Faraday cage and a vibration isolation table were used during all PDP measurements. All polarization tests were carried out for at least three replicates to ensure reproducibility of the material's corrosion behavior.

In order to minimize solution resistance and to simulate severe corrosion conditions, 3.5 wt% NaCl electrolyte made using deionized water from a Milli-Q® water purification system (18.2 MΩ cm resistivity) was chosen as the main test solution for immersion testing and standard electrochemical measurements. All measurements on bulk SS 444 and Fe were performed using a freshly polished and cleaned specimen after the sample had been immersed in the aerated test solution for 1 h. PDP measurements on thermal spray coatings and sintered pellets were performed on as received, non polished samples. Due to corrosion product accumulation in the corrosion cell, the sample and cell were washed with pure water and the electrolyte was replaced before every new PDP on immersed samples.

SECM feedback mode measurements: All C-ME characterization and SECM were performed with an ElProScan 3 system (HEKA, Germany; bipotentiostat model PG340). The polished and prepared SS 444 thermal spray coating substrate was probed using a 4.7 µm diameter carbon fiber microelectrode (C-ME), which was fabricated following an established protocol.[36] A 1 mM FcMeOH (Acros Organic, New Jersey, USA) in 0.1 M KCl (ACP, Montreal, Quebec) aqueous solution was used for all SECM measurements. The C-ME tip was polarized at 350 mV vs. SCE and the exact tip-substrate calibrated by first making contact with the surface, then retracting the tip 200 µm. The tip was then retracted and positioned 5 µm above the substrate's surface. The C-ME was rastered across the sample at 10 µm/s in order to collect the current map of the substrate. Approach curves were performed at a 1 µm/s approach speed. All measurements were performed in triplicate.

Scanning micropipette contact method: The scanning droplet cell experiment was performed over powdered SS 444 dispersed on carbon tape on a glass microscope slide. Quartz capillaries of 0.7/1.0 mm ID/OD (Sutter Instrument, Novato, CA) were pulled to form two symmetrical micropipettes with apertures of ~500 nm diameter using a P-2000 CO_2 laser puller (Sutter Instrument).

To encourage droplet stability, the exterior of the micropipettes were silanized via evaporation of dichlorodimethylsilane (Sigma-Aldrich) while passing nitrogen gas through the capillary. A silanized micropipette was filled with 3.5 wt% NaCl electrolyte. Using an established procedure, an Ag/AgCl reference wire (0.250 mm diameter Ag wire—GoodFellow Metals, Huntingdon, England), was fabricated by soaking in bleach and then wiping clean and rinsing in pure water. This was then inserted into the back of the micropipette.

With Powdered SS 444 dispersed on carbon tape acting as the working electrode, the two electrodes when in contact create the complete 2-electrode system. All SMCM PDP measurements were performed using an ElProScan 3 system (HEKA, Germany; bipotentiostat model PG340). The potential was scanned from −0.55 to ~0.15 V vs. SCE at a scan rate of 10 mV/s. The micropipette was then retracted from the substrate's surface by 100 µm, moved to the next designated area (1 µm increments), and approached towards the surface at a rate of 1 µm/s until a spike in current was measured. This measurement was carried out on 3 different samples to obtain an average E_{corr} over the passive and active regions.

DATA AVAILABILITY

The data sets generated during and/or analyzed during the current study are available from the corresponding author upon reasonable request.

ACKNOWLEDGEMENTS

The work performed was supported financially by NSERC CRD 242399, NSERC-CGS D funding, and Hydro-Québec. Authors would also like to acknowledge Nicholas Georgescu for generating the schematic in Fig. 5a and Tristan Borchers for assisting with the data collection and presentation of the Raman analysis.

AUTHOR CONTRIBUTIONS

S.M.G. performed most experiments and was the major contributor to the data analysis and manuscript preparation. I.H. carried out the ICP-OES analysis and assisted with macro PDP measurements. A.R.C.N. was responsible for the production of the HVOF coatings and pellet samples. All authors provided discussion and contributed to proof reading.

ADDITIONAL INFORMATION

Supplementary Information accompanies the paper on the *npj Materials Degradation* website (https://doi.org/10.1038/s41529-019-0087-0).

Competing interests: The authors declare no competing interests.

Publisher's note: Springer Nature remains neutral with regard to jurisdictional claims in published maps and institutional affiliations.

REFERENCES

1. Toma, D., Brandl, W. & Marginean, G. Wear and corrosion behaviour of thermally sprayed cermet coatings. *Surf. Coat. Technol.* **138**, 149–158 (2001).
2. Gärtner, F., Stoltenhoff, T., Schmidt, T. & Kreye, H. The cold spray process and its potential for industrial applications. *J. Therm. Spray. Technol.* **15**, 223–232 (2006).
3. Canadian Hydropower Association. 5 things you need to know about hydropower: Canada's number one electricity source. (2019). https://canadahydro.ca/facts Accessed January 27, 2019.
4. Liu, W.-H., Shieu, F.-S. & Hsiao, W.-T. Enhancement of wear and corrosion resistance of iron-based hard coatings deposited by high-velocity oxygen fuel (HVOF) thermal spraying. *Surf. Coat. Technol.* **249**, 24–41 (2014).
5. Kawakita, J., Fukushima, T., Kuroda, S. & Kodama, T. Corrosion behaviour of HVOF sprayed SUS316L stainless steel in seawater. *Corros. Sci.* **44**, 2561–2581 (2002).
6. Bard, A. J., Stratmann, M. & Frankel, G. S. *Encyclopedia of Electrochemistry, Volume 4, Corrosion and Oxide Films*, Wiley-VCH Verlag GmbH in Weinheim, Germany (2003).
7. Macdonald, D. D. Passivity—the key to our metals-based civilization. *Pure Appl. Chem.* **71**, 951–978 (1999).
8. Soltis, J. Passivity breakdown, pit initiation and propagation of pits in metallic materials—review. *Corros. Sci.* **90**, 5–22 (2015).
9. Jun, J., Holguin, K. & Frankel, G. S. Pitting corrosion of very clean type 304 stainless steel. *Corrosion* **70**, 146–155 (2014).
10. Koga, G. Y. et al. Microstructure and wear behavior of Fe-based amorphous HVOF coatings produced from commercial precursors. *Surf. Coat. Technol.* **309**, 938–944 (2017).
11. Ahmed, N., Bakare, M. S., McCartney, D. G. & Voisey, K. T. The effects of microstructural features on the performance gap in corrosion resistance between bulk and HVOF sprayed Inconel 625. *Surf. Coat. Technol.* **204**, 2294–2301 (2010).
12. Gateman, S. M. et al. The role of titanium in the initiation of localized corrosion of stainless steel 444. *npj Mater. Degrad.* **2**, 5 (2018).
13. Johnson, L., Niaz, A., Boatwright, A., Voisey, K. T. & Walsh, D. A. Scanning electrochemical microscopy at thermal sprayed anti-corrosion coatings: effect of thermal spraying on heterogeneous electron transfer kinetics. *J. Electroanal. Chem.* **657**, 46–53 (2011).
14. Bellezze, T., Roventi, G., Quaranta, A. & Fratesi, R. Improvement of pitting corrosion resistance of AISI 444 stainless steel to make it a possible substitute for AISI 304L and 316L in hot natural waters. *Mater. Corros.* **59**, 727–731 (2008).
15. Morita, R. et al. Corrosion resistance of TiN coatings produced by various dry processes. *Surf. Coat. Technol.* **136**, 207–210 (2001).
16. Ibrahim, M. A. M., Korablov, S. F. & Yoshimura, M. Corrosion of stainless steel coated with TiN, (TiAl)N and CrN in aqueous environments. *Corros. Sci.* **44**, 815–828 (2002).
17. Stephens, L. I. et al. Development of a model for experimental data treatment of diffusion and activation limited polarization curves for magnesium and steel alloys. *J. Electrochem. Soc.* **164**, E3576–E3582 (2017).
18. ASTM International. ASTM G61-86(2014), standard test method for conducting cyclic potentiodynamic polarization measurements for localized corrosion susceptibility of iron, nickel, or cobalt-based alloys. *J. ASTM Int.* (2014). https://doi.org/10.1520/G0061.
19. Wang, S. et al. In TMS 2018 147th Annual Meeting & Exhibition Supplemental Proceedings (ed M. & Materials Society The Minerals) 13–20, (Springer International Publishing, Cham 2018).
20. Tuan, N. T., Park, J., Lee, J., Gwak, J. & Lee, D. Synthesis of nanoporous Cu films by dealloying of electrochemically deposited Cu–Zn alloy films. *Corros. Sci.* **80**, 7–11 (2014).
21. Cornell, R. M. & Schwertmann, U. In The Iron Oxides, 2nd edition, Wiley-VCH Verlag GmbH & Co. KGaA (Weinheim, Germany 2003).
22. Brown, D. A., Cunningham, D. & Glass, W. K. The infrared and Raman spectra of chromium (III) oxide. *Spectrochim. Acta Part A Mol. Spectrosc.* **24**, 965–968 (1968).
23. Beattie, I. R. & Gilson, T. R. The single-crystal Raman spectra of nearly opaque materials. Iron(III) oxide and chromium(III) oxide. *J. Chem. Soc. A* 980–986 (1970). https://doi.org/10.1039/J19700000980.
24. Bitondo, C., Bossio, A., Monetta, T., Curioni, M. & Bellucci, F. The effect of annealing on the corrosion behaviour of 444 stainless steel for drinking water applications. *Corros. Sci.* **87**, 6–10 (2014).
25. Karlsson, H., Nyborg, L. & Berg, S. Surface chemical analysis of prealloyed water atomised steel powder. *Powder Metall.* **48**, 51–58 (2005).
26. Kim, J. K., Kim, Y. H., Lee, B. H. & Kim, K. Y. New findings on intergranular corrosion mechanism of stabilized stainless steels. *Electrochim. Acta* **56**, 1701–1710 (2011).
27. UGINE & ALZ, UGINOX F18MT: Niobium-titanium stabilized molybdenum containing 18% chromium ferritic stainless steel (Saint-Denis, France, 2005).
28. Pierson, H. O. In Handbook of Refractory Carbides and Nitrides 1–360 (Noyes Publications Albuquerque, New Mexico, 1996).
29. Pardo, A. et al. Influence of Ti, C and N concentration on the intergranular corrosion behaviour of AISI 316Ti and 321 stainless steels. *Acta Mater.* **55**, 2239–2251 (2007).
30. Jargelius-Pettersson, R. F. A. & Pound, B. G. Examination of the role of molybdenum in passivation of stainless steels using AC impedance spectroscopy. *J. Electrochem. Soc.* **145**, 1462–1469 (1998).
31. Pardo, A. et al. Pitting corrosion behaviour of austenitic stainless steels—combining effects of Mn and Mo additions. *Corros. Sci.* **50**, 1796–1806 (2008).

32. Spencer, K. & Zhang, M.-X. Optimisation of stainless steel cold spray coatings using mixed particle size distributions. *Surf. Coat. Technol.* **205**, 5135–5140 (2011).
33. AL-Mangour, B., Mongrain, R., Irissou, E. & Yue, S. Improving the strength and corrosion resistance of 316L stainless steel for biomedical applications using cold spray. *Surf. Coat. Technol.* **216**, 297–307 (2013).
34. Sova, A., Grigoriev, S., Okunkova, A. & Smurov, I. Cold spray deposition of 316L stainless steel coatings on aluminium surface with following laser post-treatment. *Surf. Coat. Technol.* **235**, 283–289 (2013).
35. Hedberg, Y., Virtanen, S. & Odnevall Wallinder, I. Micro-capillary electrochemical and microscopic investigations of massive and individual micrometer-sized powder particles of stainless steel 316L. *Int. J. Electrochem. Sci.* **7**, 11678–11695 (2012).
36. Danis, L., Polcari, D., Kwan, A., Gateman, S. M. & Mauzeroll, J. Fabrication of carbon, gold, platinum, silver, and mercury ultramicroelectrodes with controlled geometry. *Anal. Chem.* **87**, 2565–2569 (2015).